ADVANCED QUANTUM TECHNOLOGIES
www.advquantumtech.com

# Spatial Mode Correction of Single Photons Using Machine Learning

*Narayan Bhusal,* Sanjaya Lohani, Chenglong You,* Mingyuan Hong, Joshua Fabre, Pengcheng Zhao, Erin M. Knutson, Ryan T. Glasser, and Omar S. Magaña-Loaiza*

**Spatial modes of light constitute valuable resources for a variety of quantum technologies ranging from quantum communication and quantum imaging to remote sensing. Nevertheless, their vulnerabilities to phase distortions, induced by random media, impose significant limitations on the realistic implementation of numerous quantum-photonic technologies. Unfortunately, this problem is exacerbated at the single-photon level. Over the last two decades, this challenging problem has been tackled through conventional schemes that utilize optical nonlinearities, quantum correlations, and adaptive optics. In this article, the self-learning and self-evolving features of artificial neural networks are exploited to correct the complex spatial profile of distorted Laguerre–Gaussian modes at the single-photon level. Furthermore, the potential of this technique is used to improve the channel capacity of an optical communication protocol that relies on structured single photons. The results have important implications for real-time turbulence correction of structured photons and single-photon images.**

## 1. Introduction

Spatially structured beams of light have been extensively used over the last two decades for multiple applications ranging from 3D surface imaging to quantum cryptography.[1–3] In this regard, Laguerre–Gaussian (LG) modes represent an important family of spatial modes possessing orbital angular momentum (OAM).[4] The OAM of photons is due to a helical phase front given by an azimuthal phase dependence of the form $e^{i\ell\phi}$, where $\ell$ represents the OAM number and $\phi$ represents the azimuthal angle. These beams have enabled the encoding of many bits of information in a single photon, a possibility that has enabled new communication and encryption protocols.[5–11] In the past, these optical modes have been exploited to demonstrate high-speed communication in fiber, free space, and underwater.[12,13] Furthermore, structured light beams have enabled increased levels of security against eavesdroppers, a crucial feature for secure communication applications.[6,14–17] Last but not least, structured spatial profiles of single photons have been proven to be extremely useful for remote sensing technologies and correlated imaging.[18–28]

Unfortunately, the spatial profile of photons can be easily distorted in realistic environments.[29] Indeed, random phase distortions and scattering effects can destroy information encoded in structured beams of light.[30–32] Consequently, these spatial distortions severely degrade the performance of protocols for communication, cryptography, and remote sensing.[7,17] These problems are exacerbated at the single-photon level, imposing important limitations on the realistic implementation of quantum-photonic technologies. Hitherto, these limitations have been alleviated through conventional schemes that use adaptive optics, quantum correlations, and nonlinear optics.[30,33–35] However, an efficient and fast protocol to overcome undesirable turbulence effects, at the single-photon level, has not yet been experimentally demonstrated.

Recently, artificial intelligence has gained popularity in optics due to its unique potential for handling complex classification and optimization tasks.[36–43] Indeed, machine learning has been used to engineer quantum states of light,[44,45] and to identify their properties in different degrees of freedom.[46,47] The use of machine learning is rapidly growing in multiple areas like quantum state tomography, quantum metrology, and optical communication.[48–51] Moreover, convolutional neural networks (CNNs) have been demonstrated to be efficient in learning and characterizing the topographical features of images.[52] An important number of recent articles have demonstrated the potential of artificial neural networks for efficient pattern recognition and identification of spatial modes.[53,54] In addition to mode classification, artificial intelligence has enabled spatial mode

N. Bhusal, Dr. C. You, M. Hong, J. Fabre, Prof. O. S. Magaña-Loaiza
Quantum Photonics Laboratory
Department of Physics and Astronomy
Louisiana State University
Baton Rouge, LA 70803, USA
E-mail: nbhusa1@lsu.edu; cyou2@lsu.edu
Dr. S. Lohani, Dr. E. M. Knutson, Prof. R. T. Glasser
Tulane University
New Orleans LA 70118, USA
P. Zhao
School of Information Science and Technology
Qingdao University of Science and Technology
Qingdao Shandong 260061, China
The ORCID identification number(s) for the author(s) of this article can be found under https://doi.org/10.1002/qute.202000103



**DOI: 10.1002/qute.202000103**

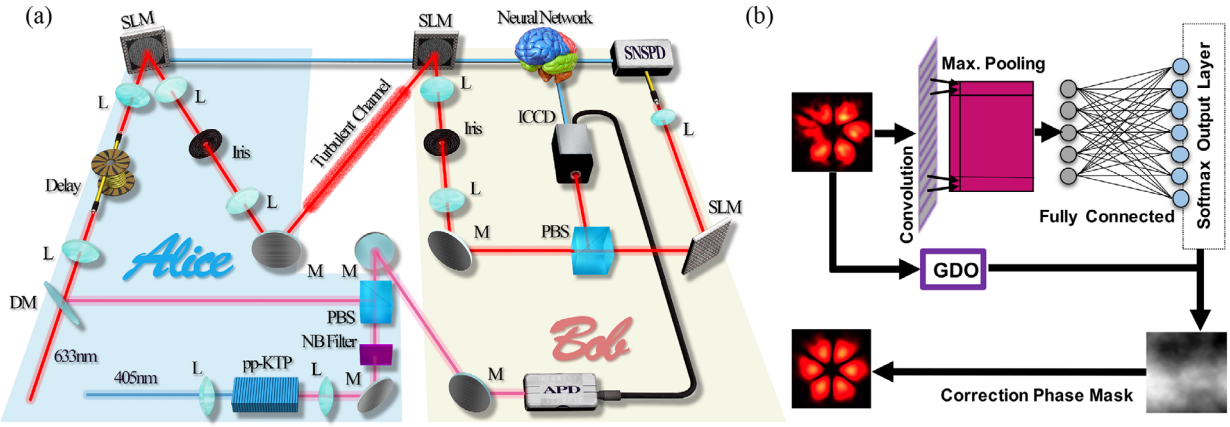


**Figure 1.** a) The schematic diagram of the setup used to demonstrate turbulence correction. The experiment is performed using a He-Ne laser and heralded single photons produced through a process of spontaneous parametric down-conversion (SPDC). The sources are switched using a dichroic mirror (DM). The spatial profile of photons is shaped by Alice using a spatial light modulator (SLM). The prepared photons are sent to Bob through a turbulent channel. Bob then performs correction and quantum state tomography on the structured photons. In order to do this, Bob collects multiple classical and single-photon images to train an artificial neural network. The high-light-level images are obtained with a CCD camera, whereas single-photon images are formed on a gated ICCD camera. b) The neural network for turbulence correction comprises a five-layer convolutional neural network (CNN), and a feedback loop with a gradient descent optimization (GDO) algorithm.

de-multiplexing, which is important for harnessing multiple bits of information per photon.[55,56] Furthermore, the self-evolving and self-learning features of artificial neural networks have been exploited to prepare, classify, and characterize quantum optical systems. Remarkably, for these particular tasks, machine learning techniques have outperformed conventional approaches.[57–60]

Here, we experimentally demonstrate a smart communication protocol that exploits the self-learning features of CNNs to correct the spatial profile of single photons. The robustness and efficiency of our scheme is tested in a communication protocol that utilizes LG modes. Our results dramatically outperform previous protocols that rely on conventional adaptive optics.[30–33] Furthermore, we demonstrate near-unity corrected fidelity in time periods that are comparable to the fluctuation of atmospheric turbulence. Our results have significant implications for various technologies that exploit single photons with complex spatial profiles.[5–7,61] In addition, our work shows an enormous potential to enable the possibility of overcoming phase distortions induced by thick atmospheric turbulence in real time.

## 2. Experimental and Computational Methods

The schematic diagram of our communication protocol and the computational model of our artificial neural network are depicted in **Figure 1**. Here, Alice prepares spatial modes that are transmitted to Bob through a turbulent communication channel. The atmospheric turbulence in the communication channel induces aberrations in the optical beams that degrade the quality of the information encoded in their phase. This undesirable effect compromises Bob's ability to correctly decode and make measurements on the spatial modes. Bob overcomes this problem by training an artificial neural network with multiple turbulence-distorted beams that allow him to correct the spatial profile of photons.

In our experiment, we use a spatial light modulator (SLM) and computer-generated holograms to produce LG modes.[62] This technique allows us to generate any arbitrary spatial mode in the first-diffraction order of the SLM. The generated modes are filtered and collimated using a 4f-optical system and then projected onto a second SLM. We use this second spatial modulator to display random phase screens that simulate turbulence.[30] The beam reflected by the second SLM is then split into two beams using a polarizing beam splitter (PBS). The spatial profile of the beams reflected by the PBS are recorded by a CCD camera. Bob collects 50 distorted modes for one specific superposition of spatial modes transmitted through a turbulent channel. The communication channel is characterized by a standard refractive index $C_n^2$. Then, 45 of these images are used as a training set and the remaining 5 are used as a test set. Each of the experimental images has a resolution of 400 × 400 pixels, then each image is downsampled to form a matrix of 128 × 128 pixels before the CNN. Once the neural network is optimized, Bob utilizes the CNN to predict the turbulence strength and the initial correction phase masks. The initial phase masks are then optimized by minimizing the mean-squared error (MSE) using the gradient descent optimization (GDO) algorithm. Furthermore, Bob utilizes the same correction masks for the single-photon and high-light-level implementation of our protocol. This is possible given the fact that the turbulence of the communication channel is independent of the number of transmitted photons. Naturally, turbulence characterization using single photons requires longer integration times. Furthermore, the beam transmitted by the PBS is characterized through quantum state tomography.

Over the past two decades, the possibility of performing image correction at the single-photon level has represented one of the main goals of the quantum imaging community.[5] Due to the relevance of single-photon imaging for multiple applications,[5,25–27,63] we also perform a proof-of-principle experiment using heralded single photons produced by a process of spontaneous parametric down-conversion (SPDC). This configuration allows us to demonstrate the potential of our turbulence correction protocol (TCP) at the single-photon level. For this purpose, we utilize a dichroic mirror (DM) to ease the

transition from one source to another as shown in Figure 1a. We produce SPDC photons by pumping a type-II potassium titanyl phosphate (ppKTP) crystal with a continuous wave (CW) diode laser at 405 nm. A PBS is used to separate the correlated photon pairs at 810 nm. We utilize temporal correlations to acquire gated images at the single-photon level using an intensified charged coupled device (ICCD) camera. This is performed by adding a delay line to our experiment. Gating the ICCD camera is crucial for the formation of single-photon images.[64]

Figure 1b illustrates our machine learning algorithm for the correction of structured photons. This is based on a CNN followed by a gradient descent optimizer.[59,65] The optimizer consists of a five-layer CNN and a GDO algorithm. The CNN takes turbulent images of LG beams, and convolves them with a $5 \times 5$ filter. The step is immediately followed by a $2 \times 2$ max-pooling layer before feeding them into 100 fully connected neurons. Finally, the network contains a softmax output layer. We utilize hundreds of instances of distorted images for multiple turbulence strengths to train the neural networks. The function of the trained CNN is to predict the strength of turbulence in terms of standard refractive index ($C_n^2$) values. The function of the GDO loop is to optimize the correction phase masks over many realizations of random matrices that simulate turbulence. The phase masks are then encoded in the second SLM to obtain the corrected spatial modes at the image plane of the SLM.

We prepare symmetric superpositions of LG modes to demonstrate smart optical communication. This family of modes are solutions to the Helmholtz equation in cylindrical coordinates.[5] Moreover, these modes form a complete orthonormal basis set with respect to the azimuthal ($\ell$) and the radial ($p$) degrees of freedom.[66] In our experiment, we distort the communication modes by using atmospheric turbulence simulated in a SLM.[67] We use the Kolmogorov model of turbulence to simulate the turbulent communication channel.[30,59,68] Turbulence induces a random modulation of the index of refraction that results from inhomogeneities of temperature and pressure of media. This, in turn, leads to distortions of the phase front of the spatial profile of optical modes. The degree of distortion is quantified through the Fried's parameter $r_0$, which is defined in terms of the standard refractive index $C_n^2$

$$\Phi(p,q) = \mathbb{R}\left\{\mathcal{F}^{-1}\left(\mathbb{M}_{NN}\sqrt{\phi_{NN}(k)}\right)\right\} \tag{1}$$

with $\phi_{NN}(k) = 0.023 r_0^{-5/3}(k^2 + k_0^2)^{-11/6} e^{-k^2/k_m^2}$ and the Fried's parameter $r_0 = (0.423 k^2 C_n^2 d)^{-3/5}$. The mathematical symbol $\mathbb{R}$ represents the real part of the complex field, whereas $\mathcal{F}^{-1}$ indicates the inverse Fourier transform operation. Furthermore, $k$, $d$, and $\mathbb{M}_{NN}$ denote the wave number ($2\pi/\lambda$), the propagation distance, and the encoded random matrix, respectively. Even though the strength of phase distortion can be varied using $d$ and $C_n^2$, we choose to vary its strength using $C_n^2$. Furthermore, we perform the phase mask optimization iteratively using the GDO algorithm

$$\Phi^j(p,q) = \angle\left[\mathcal{F}^{-1}\left\{\frac{1}{H} \times \mathcal{F}[\mathcal{F}^{-1}(\mathcal{F}(G(p,q,w_0) \times \exp(i\Theta^{(\ell,-\ell)})) \times H)\exp(-i\Phi^j_{\text{est}}(p,q))]\right\}\right] \tag{2}$$

The MSE between the predicted intensity and the corresponding simulated target intensity is used as the cost function. In this case, the symbol $\angle$ represents the complex phase defined by $\arctan(\mathbb{I}/\mathbb{R})$, with $\mathbb{I}$ describing the imaginary part of the complex field. Moreover, $\mathcal{F}$ indicates a Fourier transform operation, and $\Phi^j(p,q)$ the phase mask at the $j$th iteration. The Gaussian beam $G(p,q,w_0)$ is characterized by a waist $w_0$, and the transfer function describing the SLM transformation together with the propagation function of the beam is represented by $H$. The phase mask used to generate the original LG superposition mode is described by $\Theta^{(\ell,-\ell)}$ in Equation (2).

## 3. Results and Discussion

In **Figure 2**a–c, we present experimental results obtained with a He-Ne laser. The first column in each of the panels shows the spatial profile of the undistorted modes prepared by Alice. The spatial profiles of the modes are distorted due to atmospheric turbulence in the communication channel. The aberrated modes are shown in the second column of Figure 2. In the experiment, Bob collects hundreds of realizations of the aberrated beams to train the artificial neural network in Figure 1b. The strength of turbulence predicted by our CNN was utilized to perform the phase mask optimization by means of a feedback GDO loop. Thus, the CNN in combination with the GDO loop generate the correction phase masks which are then encoded in the second SLM to alleviate turbulence effects. We indicate this process with the blue box labeled as "TCP" in Figure 2. The CNN was trained in a high-performance computing cluster. The pre-trained CNNs are used to estimate the turbulence strength and initial phase distribution in few milliseconds. The pre-trained CNNs and GDO are run in a computer with an Intel(R) Core(TM) i7-8750H CPU @ 2.20 GHz and 16 GB of RAM to generate optimized turbulence correction phase masks. In order to show the performance of our artificial neural network, in **Figure 3** we plot the MSE as a function of the iteration number. This plot allows for a qualitative comparison of our protocol with other adaptive optics techniques.[30,69] Naturally, the number of iterations required for convergence depends on the strength of turbulence. Our protocol shows a similar performance to other adaptive optics protocols, see [30, 69]. Nevertheless, the standard refractive index ($C_n^2$) values are orders of magnitude higher. The MSE starts to converge near 100 iterations for the turbulence strengths used in the experiment, see Figure 3. This process enables Bob to obtain optimized phase masks which are used to correct turbulence-induced distortions. The corrected intensity profiles measured by Bob are depicted in the last column of each panel in Figure 2. In Figure 2a, we show the spatial profile of a structured beam corrected by our protocol for the superposition of LG modes $|\psi\rangle = \frac{1}{\sqrt{2}}(|\text{LG}_{+\ell,0}\rangle + |\text{LG}_{-\ell,0}\rangle)$ with $\ell = 5$. In Figure 2b,c, we show experimental results for complex LG modes, with radial structure, described by $|\psi\rangle = \frac{1}{\sqrt{2}}(|\text{LG}_{+\ell,1}\rangle + |\text{LG}_{-\ell,1}\rangle)$ for $\ell = 3$ and $\ell = 5$, respectively.

We also demonstrate the robustness of our technique to correct the spatial profile of heralded single photons. In Figure 2d–f, we display turbulence correction of single photons prepared in LG superpositions with different azimuthal and radial quantum numbers, expressed as $|\psi\rangle = \frac{1}{\sqrt{2}}(|\text{LG}_{+5,0}\rangle + |\text{LG}_{-5,0}\rangle)$, $|\psi\rangle = \frac{1}{\sqrt{2}}(|\text{LG}_{+3,1}\rangle + |\text{LG}_{-3,1}\rangle)$,

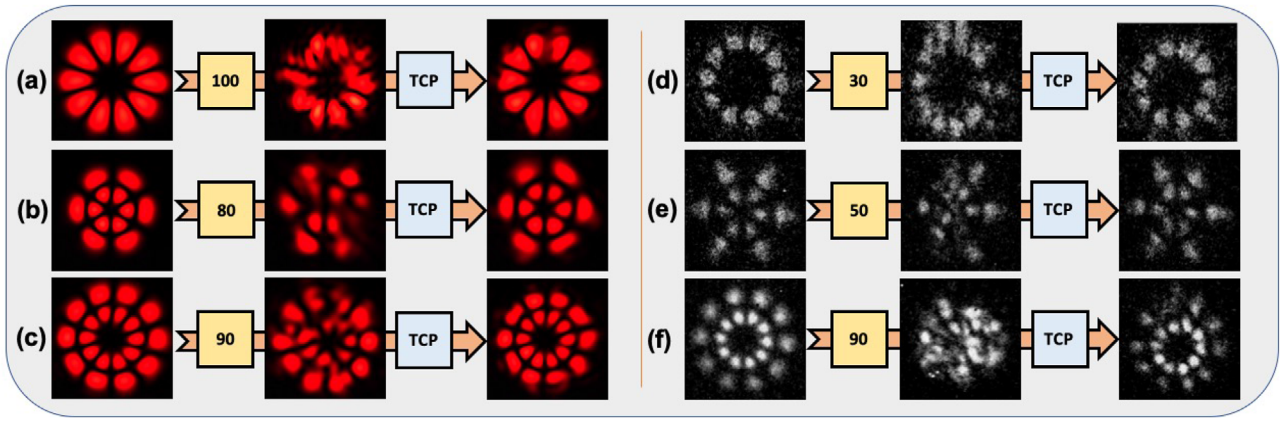


**Figure 2.** Spatial profiles of LG modes at high- and single-photon levels for different turbulence conditions. The first column in each of the panels shows the states prepared by Alice without distortions. The second columns display the distorted beams measured by Bob. The strength of turbulence is characterized by $C_n^2$ ($\times 10^{-13}\,\mathrm{mm}^{-2/3}$), these numbers are reported in the yellow rectangle. The spatial profiles after our turbulence correction protocol (TCP) are shown in the third column. a–c) High-light-level demonstrations of our protocol for multiple LG superpositions, $|\psi\rangle = \frac{1}{\sqrt{2}}(|\mathrm{LG}_{+5,0}\rangle + |\mathrm{LG}_{-5,0}\rangle)$, $|\psi\rangle = \frac{1}{\sqrt{2}}(|\mathrm{LG}_{+3,1}\rangle + |\mathrm{LG}_{-3,1}\rangle)$, and $|\psi\rangle = \frac{1}{\sqrt{2}}(|\mathrm{LG}_{+5,1}\rangle + |\mathrm{LG}_{-5,1}\rangle)$, respectively. d–f) The corresponding single-photon demonstrations of (a), (b), and (c), respectively.

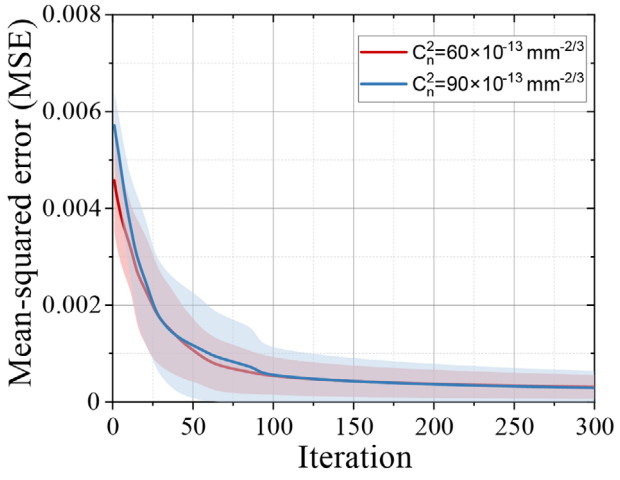


**Figure 3.** Mean-squared error (MSE) versus the iteration number in GDO. The red and blue lines indicate the MSE values for turbulence strengths $C_n^2 = 60\times10^{-13}$ and $90\times10^{-13}$ $\mathrm{mm}^{-2/3}$, respectively. The number of iterations needed for the algorithm to achieve convergence depends on the strength of turbulence. In general, stronger turbulence requires longer times to converge.

and $|\psi\rangle = \frac{1}{\sqrt{2}}(|\mathrm{LG}_{+5,1}\rangle + |\mathrm{LG}_{-5,1}\rangle)$, respectively. These images were acquired using an ICCD camera. Each of the background-subtracted images are formed by accumulating photons over a time period of 20 min. These images demonstrate an excellent mitigation of the turbulence at the single-photon level. It is important to note that the implementation of the protocol in real time is the ultimate goal. However, we would like to emphasize the fact that speed and collection time in our experiment are limited by our computational resources and the performance of our equipment. Thus, the overall reported speed in our manuscript is not a fundamental constraint nor a problem of our protocol. Indeed, it is possible to speed-up our scheme by replacing our commercial ICCD camera with a fast single-photon camera with nanosecond resolution such as the one described in ref. [70].

We quantify the performance of our correction protocol through the channel capacity of our optical communication system. **Figure 4**a shows the cross-correlation matrix for different transmitted modes in the absence of turbulence. In order to generate this matrix, Bob performs a series of projective measurements on the modes sent by Alice. The cross-correlation matrix represents the conditional probabilities between the modes sent and detected in the communication protocol. A small spread around the diagonal elements even in the absence of turbulence is caused due to diffraction, the finite size of the optical fibers, and experimental misalignment. The cross-correlation matrix obtained in the presence of atmospheric turbulence is shown in Figure 4b. In this case, the spatial distortion induces modal crosstalk that degrades the performance of the communication protocol. These undesirable effects increase with the strength of turbulence in the communication channel. Indeed, this represents an important limitation of free-space communication with spatial modes of light.[5] In Figure 4c, we show our experimental results for the cross-correlation matrix after applying our turbulence correction protocol. In this case, the cross-correlation matrix is nearly diagonal, showing a dramatic improvement in the performance of our communication protocol. Furthermore, we calculate the normalized mutual information to quantify the channel capacity in terms of bits per photon[30] as shown in Figure 4d. We used the conditional probabilities of the cross-correlation matrices to calculate the mutual information for a high-dimensional Hilbert space according to the following equation $\mathrm{MI} = \frac{1}{N}\sum_{d,s} P(d \mid s)\log_2\left(\frac{P(d|s)N}{\sum_s P(d|s)}\right)$, where the dimension is described by the parameter $N$, and the subscripts $d$ and $s$ represent the detected and sent modes, respectively. Here, $P(d \mid s)$ denotes the conditional probability of detecting the state in spatial mode $d$, given mode $s$ is sent by Alice. The channel capacity plot demonstrates the potential of our technique to correct spatial modes of light.

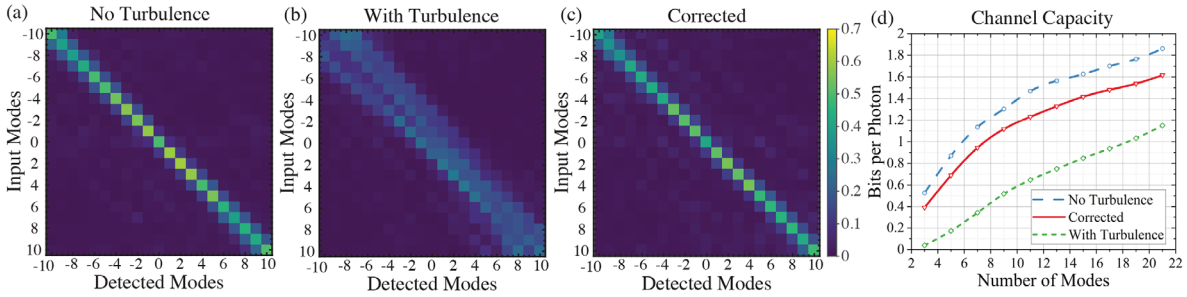


**Figure 4.** The cross-correlation matrices represent conditional probabilities between sent and detected modes in the OAM basis. a) The cross-correlation matrix obtained for our communication protocol in the absence of turbulence. b) Plot of the cross-correlation matrix in the presence of turbulence characterized by $C_n^2 = 90{\times}10^{-13}$ mm$^{-2/3}$. In this case, it is almost impossible to correctly identify the spatial modes. c) The cross-correlation matrix after applying our turbulence correction protocol. Our turbulence correction protocol significantly improves the performance of the communication system. d) Channel capacity in terms of bits per photon.

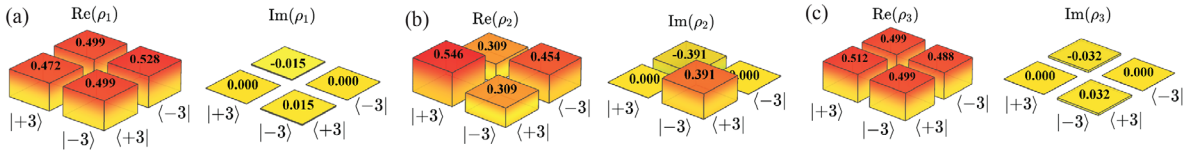


**Figure 5.** Real and imaginary parts of the density matrices for the qubits encoded in the OAM basis. In this case, we prepared $|\psi_3\rangle = \frac{1}{\sqrt{2}}(|\mathrm{LG}_{+3,0}\rangle + |\mathrm{LG}_{-3,0}\rangle)$. a) The real and imaginary parts of the density matrix for the undistorted state. b) The density matrix for the aberrated qubit. In this case, the strength of the simulated turbulence is characterized by $C_n^2 = 80{\times}10^{-13}$ mm$^{-2/3}$. c) The density matrix for the corrected qubit after applying our turbulence correction protocol. We measured a fidelity of 99.9% for the prepared state, 81.7% for the distorted state, and 99.8% for the state corrected through our machine learning protocol.

In order to certify the spatial correction of single photons and the recovery of spatial coherence, we perform quantum state tomography of the spatial modes.[63] For this purpose we use superpositions of the following form, $|\psi_\ell\rangle = \alpha\,|\mathrm{LG}_{+\ell,0}\rangle + \beta\,|\mathrm{LG}_{-\ell,0}\rangle$, where $\alpha$, and $\beta$ represent complex amplitudes.[67,71–73] For simplicity, in our experiment we use the following spatial qubit $|\psi_3\rangle = \frac{1}{\sqrt{2}}(|\mathrm{LG}_{+3,0}\rangle + |\mathrm{LG}_{-3,0}\rangle)$. In **Figure 5**a–c, we show the real and imaginary parts of the reconstructed density matrices in the absence of turbulence, with turbulence, and after applying turbulence correction, respectively. As shown in Figure 5a, in this case, all the elements of the real part of the density matrix should be equal to 1/2, and the matrix elements of the imaginary part should be 0. The presence of any deviation from that is attributed to experimental imperfections. Furthermore, Figure 5b shows the detrimental effects produced by turbulence. The strength of turbulence in this case is $C_n^2 = 80{\times}10^{-13}$ mm$^{-2/3}$. After applying our machine learning protocol, we recover the original state almost perfectly. The shown density matrices certify the robustness of our technique. We quantify the fidelity using $\mathcal{F} = (\mathrm{Tr}\sqrt{\sqrt{\rho_1}\rho_3\sqrt{\rho_1}})^2$, where $\rho_1$ and $\rho_3$ represent the density matrices of the original and turbulence corrected spatial qubits. The measured fidelity for the prepared state is 99.9%, whereas that of the distorted state is 81.7%. Remarkably, the fidelity for the state corrected through our machine learning protocol is 99.8%.

## 4. Conclusion

Spatial photonic modes have been in the spotlight for the past few decades due to their enormous potential as quantum information resources. However, these modes are fragile and vulnerable to random phase fluctuations induced by turbulence. Unfortunately, these problems are exacerbated at the single-photon level. The fragility of spatial modes of photons imposes important limitations on the realistic implementation of optical technologies in free space. In this work, we have experimentally demonstrated the first smart communication protocol that exploits the self-learning features of CNNs to correct the spatial profile of single photons. This work represents a significant improvement over conventional schemes for turbulence correction.[30,33] [69] The high fidelities achieved in the reconstruction of the spatial profile of single photons make our technique a robust tool for free-space quantum technologies. We believe that our work has important implications for the realistic implementation of photonic quantum technologies.

## Acknowledgements

N.B. and O.S.M.-L. would like to acknowledge the financial support from Army Research Office (ARO) under grant no. W911NF-20-1-0194. C.Y., J.F., and O.S.M.-L. are supported by the U.S. Department of Energy, Office of Basic Energy Sciences, Division of Materials Sciences and Engineering under Award DE-SC0021069. R.T.G. acknowledges funding from the U.S. Office of Naval Research under grant number N000141912374.

## Conflict of Interest

The authors declare no conflict of interest.

## Keywords

machine learning, optical communication, single-photon imaging, structured light, turbulence

Received: September 16, 2020
Revised: December 22, 2020
Published online: January 22, 2021

[1] H. Rubinsztein-Dunlop, A. Forbes, M. V. Berry, M. R. Dennis, D. L. Andrews, M. Mansuripur, C. Denz, C. Alpmann, P. Banzer, T. Bauer, E. Karimi, L. Marrucci, M. Padgett, M. Ritsch-Marte, N. M. Litchinitser, N. P. Bigelow, C. Rosales-Guzmán, A. Belmonte, J. P. Torres, T. W. Neely, M. Baker, R. Gordon, A. B. Stilgoe, J. Romero, A. G. White, R. Fickler, A. E. Willner, G. Xie, B. McMorran, A. M. Weiner, *J. Opt.* **2016**, *19*, 013001.
[2] T. Bell, B. Li, S. Zhang, *Wiley Encyclopedia of Electrical and Electronics Engineering*, Wiley, Hoboken, NJ **1999**, pp. 1–24.
[3] J. Geng, *Adv. Opt. Photon.* **2011**, *3*, 128.
[4] D. L. Andrews, M. Babiker, *The Angular Momentum of Light*, Cambridge University Press, Cambridge **2012**.
[5] O. S. Magaña-Loaiza, R. W. Boyd, *Rep. Prog. Phys.* **2019**, *82*, 124401.
[6] A. E. Willner, H. Huang, Y. Yan, Y. Ren, N. Ahmed, G. Xie, C. Bao, L. Li, Y. Cao, Z. Zhao, J. Wang, M. P. J. Lavery, M. Tur, S. Ramachandran, A. F. Molisch, N. Ashrafi, S. Ashrafi, *Adv. Opt. Photon.* **2015**, *7*, 66.
[7] A. M. Yao, M. J. Padgett, *Adv. Opt. Photon.* **2011**, *3*, 161.
[8] J. Wang, J.-Y. Yang, I. M. Fazal, N. Ahmed, Y. Yan, H. Huang, Y. Ren, Y. Yue, S. Dolinar, M. Tur, A. E. Willner, *Nature Photon.* **2012**, *6*, 488.
[9] G. Milione, M. P. Lavery, H. Huang, Y. Ren, G. Xie, T. A. Nguyen, E. Karimi, L. Marrucci, D. A. Nolan, R. R. Alfano, A. E. Willner, *Opt. Lett.* **2015**, *40*, 1980.
[10] M. Erhard, R. Fickler, M. Krenn, A. Zeilinger, *Light Sci. Appl.* **2018**, *7*, 17146.
[11] T. Giordani, E. Polino, S. Emiliani, A. Suprano, L. Innocenti, H. Majury, L. Marrucci, M. Paternostro, A. Ferraro, N. Spagnolo, F. Sciarrino, *Phys. Rev. Lett.* **2019**, *122*, 020503.
[12] M. Krenn, J. Handsteiner, M. Fink, R. Fickler, A. Zeilinger, *Proc. Natl. Acad. Sci. USA* **2015**, *112*, 14197.
[13] J. Baghdady, K. Miller, K. Morgan, M. Byrd, S. Osler, R. Ragusa, W. Li, B. M. Cochenour, E. G. Johnson, *Opt. Express* **2016**, *24*, 9794.
[14] M. Bourennane, A. Karlsson, G. Björk, N. Gisin, N. J. Cerf, *J. Phys. A: Math. Gen.* **2002**, *35*, 10065.
[15] M. Mirhosseini, O. S. Magaña-Loaiza, M. N. O'Sullivan, B. Rodenburg, M. Malik, M. P. Lavery, M. J. Padgett, D. J. Gauthier, R. W. Boyd, *New J. Phys.* **2015**, *17*, 033033.
[16] S. Gröblacher, T. Jennewein, A. Vaziri, G. Weihs, A. Zeilinger, *New J. Phys.* **2006**, *8*, 75.
[17] M. Malik, M. O'Sullivan, B. Rodenburg, M. Mirhosseini, J. Leach, M. P. Lavery, M. J. Padgett, R. W. Boyd, *Opt. Express* **2012**, *20*, 13195.
[18] O. S. Magaña-Loaiza, M. Mirhosseini, R. M. Cross, S. M. H. Rafsanjani, R. W. Boyd, *Sci. Adv.* **2016**, *2*, e1501143.
[19] Z. Yang, O. S. Magaña-Loaiza, M. Mirhosseini, Y. Zhou, B. Gao, L. Gao, S. M. H. Rafsanjani, G.-L. Long, R. W. Boyd, *Light Sci. Appl.* **2017**, *6*, e17013.
[20] N. Cvijetic, G. Milione, E. Ip, T. Wang, *Sci. Rep.* **2015**, *5*, 15422.
[21] N. Uribe-Patarroyo, A. Fraine, D. S. Simon, O. Minaeva, A. V. Sergienko, *Phys. Rev. Lett.* **2013**, *110*, 043601.
[22] O. S. Magaña-Loaiza, R. d. J. León-Montiel, A. Perez-Leija, A. B. U'Ren, C. You, K. Busch, A. E. Lita, S. W. Nam, R. P. Mirin, T. Gerrits, *NPJ Quantum Inf.* **2019**, *5*, 80.
[23] G. Milione, T. Wang, J. Han, L. Bai, *Chin. Opt. Lett.* **2017**, *15*, 030012.
[24] M. P. Lavery, F. C. Speirits, S. M. Barnett, M. J. Padgett, *Science* **2013**, *341*, 537.
[25] L. Chen, J. Lei, J. Romero, *Light Sci. Appl.* **2014**, *3*, e153.
[26] B. Jack, J. Leach, J. Romero, S. Franke-Arnold, M. Ritsch-Marte, S. Barnett, M. Padgett, *Phys. Rev. Lett.* **2009**, *103*, 083602.
[27] M. Malik, R. Boyd, *Riv. Nuovo Cimento* **2014**, *37*, 5.
[28] G. Scarcelli, V. Berardi, Y. Shih, *Appl. Phys. Lett.* **2006**, *88*, 061106.
[29] B. Rodenburg, M. P. Lavery, M. Malik, M. N. O'Sullivan, M. Mirhosseini, D. J. Robertson, M. Padgett, R. W. Boyd, *Opt. Lett.* **2012**, *37*, 3735.
[30] B. Rodenburg, M. Mirhosseini, M. Malik, O. S. Magaña-Loaiza, M. Yanakas, L. Maher, N. K. Steinhoff, G. A. Tyler, R. W. Boyd, *New J. Phys.* **2014**, *16*, 033020.
[31] C. Paterson, *Phys. Rev. Lett.* **2005**, *94*, 153901.
[32] G. A. Tyler, R. W. Boyd, *Opt. Lett.* **2009**, *34*, 142.
[33] H. Defienne, M. Reichert, J. W. Fleischer, *Phys. Rev. Lett.* **2018**, *121*, 233601.
[34] T. A. Smith, Y. Shih, *Phys. Rev. Lett.* **2018**, *120*, 063606.
[35] A. N. Black, E. Giese, B. Braverman, N. Zollo, S. M. Barnett, R. W. Boyd, *Phys. Rev. Lett.* **2019**, *123*, 143603.
[36] X. Lin, Y. Rivenson, N. T. Yardimci, M. Veli, Y. Luo, M. Jarrahi, A. Ozcan, *Science* **2018**, *361*, 1004.
[37] V. Dunjko, H. J. Briegel, *Rep. Prog. Phys.* **2018**, *81*, 074001.
[38] Y. LeCun, Y. Bengio, G. Hinton, *Nature* **2015**, *521*, 436.
[39] J. Biamonte, P. Wittek, N. Pancotti, P. Rebentrost, N. Wiebe, S. Lloyd, *Nature* **2017**, *549*, 195.
[40] S. Adhikari, C. L. Cortes, X. Wen, S. Panuganti, D. J. Gosztola, R. D. Schaller, G. P. Wiederrecht, S. K. Gray, arXiv:2006.01904, **2020**.
[41] X.-D. Cai, D. Wu, Z.-E. Su, M.-C. Chen, X.-L. Wang, L. Li, N.-L. Liu, C.-Y. Lu, J.-W. Pan, *Phys. Rev. Lett.* **2015**, *114*, 110504.
[42] T. Giordani, A. Suprano, E. Polino, F. Acanfora, L. Innocenti, A. Ferraro, M. Paternostro, N. Spagnolo, F. Sciarrino, *Phys. Rev. Lett.* **2020**, *124*, 160401.
[43] J. Romero, A. Aspuru-Guzik, *Adv. Quantum Technol.* **2021**, *4*, 2000003.
[44] M. Krenn, M. Malik, R. Fickler, R. Lapkiewicz, A. Zeilinger, *Phys. Rev. Lett.* **2016**, *116*, 090405.
[45] C. Cui, R. Arian, S. Guha, N. Peyghambarian, Q. Zhuang, Z. Zhang, *Phys. Rev. Appl.* **2019**, *12*, 034059.
[46] J. Gao, L.-F. Qiao, Z.-Q. Jiao, Y.-C. Ma, C.-Q. Hu, R.-J. Ren, A.-L. Yang, H. Tang, M.-H. Yung, X.-M. Jin, *Phys. Rev. Lett.* **2018**, *120*, 240501.
[47] C. You, M. A. Quiroz-Juárez, A. Lambert, N. Bhusal, C. Dong, A. Perez-Leija, A. Javaid, R. d. J. León-Montiel, O. S. Magaña-Loaiza, *Appl. Phys. Rev.* **2020**, *7*, 021404.
[48] E. Polino, M. Valeri, N. Spagnolo, F. Sciarrino, *AVS Quantum Sci.* **2020**, *2*, 024703.
[49] G. Torlai, G. Mazzola, J. Carrasquilla, M. Troyer, R. Melko, G. Carleo, *Nature Phys.* **2018**, *14*, 447.
[50] G. Carleo, I. Cirac, K. Cranmer, L. Daudet, M. Schuld, N. Tishby, L. Vogt-Maranto, L. Zdeborová, *Rev. Mod. Phys.* **2019**, *91*, 045002.
[51] S. Lohani, E. M. Knutson, R. T. Glasser, *Commun. Phys.* **2020**, *3*, 1.
[52] J. Gu, Z. Wang, J. Kuen, L. Ma, A. Shahroudy, B. Shuai, T. Liu, X. Wang, G. Wang, J. Cai, T. Chen, *Pattern Recognit.* **2018**, *77*, 354.
[53] M. Krenn, R. Fickler, M. Fink, J. Handsteiner, M. Malik, T. Scheidl, R. Ursin, A. Zeilinger, *New J. Phys.* **2014**, *16*, 113028.
[54] M. Krenn, J. Handsteiner, M. Fink, R. Fickler, R. Ursin, M. Malik, A. Zeilinger, *Proc. Natl. Acad. Sci. USA* **2016**, *113*, 13648.
[55] T. Doster, A. T. Watnik, *Appl. Opt.* **2017**, *56*, 3386.
[56] S. R. Park, L. Cattell, J. M. Nichols, A. Watnik, T. Doster, G. K. Rohde, *Opt. Express* **2018**, *26*, 4004.
[57] A. Turpin, I. Vishniakou, J. d Seelig, *Opt. Express* **2018**, *26*, 30911.
[58] S. Lohani, E. M. Knutson, M. O'Donnell, S. D. Huver, R. T. Glasser, *Appl. Opt.* **2018**, *57*, 4180.
[59] S. Lohani, R. T. Glasser, *Opt. Lett.* **2018**, *43*, 2611.

[60] J. Liu, P. Wang, X. Zhang, Y. He, X. Zhou, H. Ye, Y. Li, S. Xu, S. Chen, D. Fan, *Opt. Express* **2019**, *27*, 16671.
[61] R.-B. Jin, W.-H. Cai, C. Ding, F. Mei, G.-W. Deng, R. Shimizu, Q. Zhou, *Quantum Eng.* **2020**, *2*, e38.
[62] A. Forbes, A. Dudley, M. McLaren, *Adv. Opt. Photon.* **2016**, *8*, 200.
[63] M. Mirhosseini, O. S. Magaña-Loaiza, C. Chen, S. M. H. Rafsanjani, R. W. Boyd, *Phys. Rev. Lett.* **2016**, *116*, 130402.
[64] R. Fickler, M. Krenn, R. Lapkiewicz, S. Ramelow, A. Zeilinger, *Sci. Rep.* **2013**, *3*, 1914.
[65] M. A. Nielsen, *Neural Networks and Deep Learning*, Determination Press, San Francisco, CA **2015**.
[66] A. E. Siegman, *Lasers*, University Science Books, Mill Valley, CA **1986**.
[67] B. Rodenburg, O. S. Magaña-Loaiza, M. Mirhosseini, P. Taherirostami, C. Chen, R. W. Boyd, *J. Opt.* **2016**, *18*, 054015.
[68] J. P. Bos, M. C. Roggemann, V. R. Gudimetla, *Appl. Opt.* **2015**, *54*, 2039.
[69] G. Xie, Y. Ren, H. Huang, M. P. Lavery, N. Ahmed, Y. Yan, C. Bao, L. Li, Z. Zhao, Y. Cao, M. Willner, M. Tur, S. J. Dolinar, R. W. Boyd, J. H. Shapiro, A. E. Willner, *Opt. Lett.* **2015**, *40*, 1197.
[70] N. Montaut, O. S. Magaña-Loaiza, T. J. Bartley, V. B. Verma, S. W. Nam, R. P. Mirin, C. Silberhorn, T. Gerrits, *Optica* **2018**, *5*, 1418.
[71] J. B. Altepeter, E. R. Jeffrey, P. G. Kwiat, *Adv. At., Mol., Opt. Phys.* **2005**, *52*, 105.
[72] D. F. James, P. G. Kwiat, W. J. Munro, A. G. White, *Phys. Rev. A* **2001**, *64*, 052312.
[73] A. Nicolas, L. Veissier, E. Giacobino, D. Maxein, J. Laurat, *New J. Phys.* **2015**, *17*, 033037.